

Typeset using L<sup>A</sup>T<sub>E</sub>X preprint style in AASTeX63

## AGILE Observations of Two Repeating Fast Radio Bursts with Small Intrinsic Dispersion Measure

C. CASENTINI,<sup>1,2</sup> F. VERRECCHIA,<sup>3,4</sup> M. TAVANI,<sup>1,5</sup> A. URSI,<sup>1</sup> L.A. ANTONELLI,<sup>4</sup> A. ARGAN,<sup>6</sup> G. BARBIELLINI,<sup>6</sup> A. BULGARELLI,<sup>7</sup> P. CARAVEO,<sup>8,9</sup> M. CARDILLO,<sup>1</sup> P.W. CATTANEO,<sup>9</sup> A. CHEN,<sup>10</sup> E. COSTA,<sup>1</sup> I. DONNARUMMA,<sup>11</sup> M. FEROCI,<sup>1</sup> A. FERRARI,<sup>12</sup> F. FUSCHINO,<sup>7</sup> M. GALLI,<sup>7,13</sup> A. GIULIANI,<sup>8</sup> C. LABANTI,<sup>7</sup> F. LAZZAROTTO,<sup>14</sup> P. LIPARI,<sup>15,16</sup> F. LONGO,<sup>6</sup> F. LUCARELLI,<sup>3,4</sup> M. MARISALDI,<sup>17</sup> A. MORSELLI,<sup>2</sup> F. PAOLETTI,<sup>18,1</sup> N. PARMIGGIANI,<sup>7</sup> A. PELLIZZONI,<sup>19</sup> G. PIANO,<sup>1</sup> M. PILIA,<sup>19</sup> C. PITTORI,<sup>3,4</sup> AND S. VERCELLONE<sup>20</sup>

<sup>1</sup>INAF/IAPS, via del Fosso del Cavaliere 100, I-00133 Roma (RM), Italy

<sup>2</sup>INFN Sezione di Roma 2, via della Ricerca Scientifica 1, I-00133 Roma (RM), Italy

<sup>3</sup>SSDC/ASI, via del Politecnico snc, I-00133 Roma (RM), Italy

<sup>4</sup>INAF/OAR, via Frascati 33, I-00078 Monte Porzio Catone (RM), Italy

<sup>5</sup>Università degli Studi di Roma Tor Vergata, via della Ricerca Scientifica 1, I-00133 Roma (RM), Italy

<sup>6</sup>Dipartimento di Fisica, Università di Trieste and INFN, via Valerio 2, I-34127 Trieste (TR), Italy

<sup>7</sup>INAF/OAS, via Gobetti 101, I-40129 Bologna (BO), Italy

<sup>8</sup>INAF/IASF, via E. Bassini 15, I-20133 Milano (MI), Italy

<sup>9</sup>INFN Sezione di Pavia, via U. Bassi 6, I-27100 Pavia (PV), Italy

<sup>10</sup>School of Physics, Wits University, Johannesburg, South Africa

<sup>11</sup>ASI, via del Politecnico snc, I-00133 Roma (RM), Italy

<sup>12</sup>CIFS presso Dipartimento di Fisica, Università di Torino, via P. Giuria 1, I-10125, Torino, Italy

<sup>13</sup>ENEA Bologna, via don Fiammelli 2, I-40128 Bologna (BO), Italy

<sup>14</sup>INAF - Osservatorio Astronomico di Padova, vicolo Osservatorio 5, I-35122 Padova (PD), Italy

<sup>15</sup>Dipartimento Fisica, Università La Sapienza, p.le Aldo Moro 2, I-00185 Roma (RM), Italy

<sup>16</sup>INFN Sezione di Roma 1, p.le Aldo Moro 2, I-00185 Roma, Italy

<sup>17</sup>Birkeland Centre for Space Science, Department of Physics and Technology, University of Bergen, Norway

<sup>18</sup>East Windsor RSD, 25A Leshin Lane, Hightstown, NJ-08520, USA

<sup>19</sup>INAF - Osservatorio Astronomico di Cagliari, via della Scienza 5, I-09047 Selargius (CA), Italy

<sup>20</sup>INAF - Osservatorio Astronomico di Brera, via E. Bianchi 46, I-23807 Merate (MI), Italy

Submitted to Astrophysical Journal Letters on Nov. 21, 2019

### ABSTRACT

Fast radio bursts (FRBs) are transient radio sources of unknown origin. Here we focus on two repeating FRBs recently detected by the CHIME/FRB experiment in 2018-2019 (Source 1: 180916.J0158+65, and Source 2: 181030.J1054+73). These

[claudio.casentini@inaf.it](mailto:claudio.casentini@inaf.it)

[francesco.verrecchia@inaf.it](mailto:francesco.verrecchia@inaf.it)

[marco.tavani@inaf.it](mailto:marco.tavani@inaf.it)

sources have small intrinsic dispersion measures (DMs), implying relatively small distances. The locations of these two sources were repeatedly observed by the AGILE instrument in the MeV-GeV energy range. We do not detect prompt emission in the MeV range simultaneously with these repeating events. This search is particularly significant for the sub-millisecond and millisecond integrations obtainable by AGILE. The sources are constrained to emit an MeV-fluence in the millisecond range below  $F'_{MeV} = 10^{-8} \text{ erg cm}^{-2}$  corresponding to an isotropic energy near  $E_{MeV,UL} \simeq 10^{40} \text{ erg}$  for an assumed distance of 100 kpc (clearly excluding emissions similar to SGR 1806-20). We also searched for  $\gamma$ -ray emission above 50 MeV for time intervals extending up to 100 days. For long timescales, we obtain upper limits (UL) for the average isotropic luminosity above 50 MeV,  $L_{\gamma,UL} \simeq (1 - 2) \cdot 10^{37} \text{ erg s}^{-1}$ . Alternately, for a source distance near 100 Mpc, our ULs imply  $E_{MeV,UL} \simeq 10^{46} \text{ erg}$  and  $L_{\gamma,UL} \simeq (1 - 2) \cdot 10^{43} \text{ erg s}^{-1}$ . Our results are significant in constraining the high-energy emission of possible underlying sources such as magnetars and show the prompt emission to be lower than the peak of the 2004 magnetar outburst of SGR 1806-20.

## 1. INTRODUCTION

Fast radio bursts (FRBs) are a new transient phenomenon of unknown origin consisting of bright millisecond radio pulses (mainly at  $\sim 1 \text{ GHz}$ ) having large dispersion measures (DM) in excess of Galactic values (Lorimer et al. 2007; Cordes & Chatterjee 2019). For most of the sources with isotropic sky distribution, a single radio burst has been detected. A smaller number of FRBs show repeating pulses which appear to occur erratically in time (see the FRB catalogue, frbcat<sup>1</sup>; Petroff et al. 2016). No clear evidence for physically different populations has been obtained.

The possible cosmological origin of a sample of FRBs was confirmed at least for one source, the first repeater FRB 121102 (Spitler et al. 2016), which was localized in a dwarf galaxy at  $z = 0.193$  ( $DM = 560 \text{ pc cm}^{-3}$ ) with a persistent radio emission (Chatterjee et al. 2017; Marcote et al. 2017). Various models have been proposed to explain the FRB radio emission which is characterized by a few-ms timescale and  $\mu\text{s}$  sub-burst structure (Champion et al. 2016; Michilli et al. 2018; Hessels et al. 2019). Possible underlying sources include compact objects such as supermassive black holes or young magnetars in young or relatively aged remnants (Metzger et al. 2019). The enigmatic nature of FRBs results from the ms timescale emission and detected fluences implying energies of radio emission near  $10^{39} \text{ erg}$  for sources at extragalactic distances. Such large energies and implied radio luminosities suggest a physical production mechanism with no analogue found in known Galactic sources.

Recently, the CHIME/FRB collaboration has reported the discovery of an additional repeating FRB, FRB 180814.J0453 (CHIME/FRB Collaboration et al. 2019a,b), and later of 8 new repeating sources (CHIME/FRB Collaboration et al. 2019c, hereafter C19) with DM ranging from  $103.5$  to  $1281 \text{ pc cm}^{-3}$ . The characteristics of this latter sample of repeating FRBs are particularly interesting for counterpart searches, as we elaborate below. High-energy counterpart searches for FRBs different

<sup>1</sup> <http://www.frbcat.org/>

from those of C19 have been recently reported (Scholz et al. 2017; Cunningham et al. 2019; Martone et al. 2019).

AGILE is a space mission of the Italian Space Agency (ASI) devoted to X and  $\gamma$ -ray astrophysics (Tavani et al. 2009), operating since 2007 in an equatorial orbit. Due to its spinning operational mode, every 7 minutes it exposes  $\sim 80\%$  of the entire sky. The instrument consists of four different detectors: an imaging  $\gamma$ -ray Silicon Tracker (sensitive in the energy range 30 MeV – 30 GeV; Barbiellini et al. 2002), an X-ray imager, Super-AGILE (Super-A, operating in the energy range 20 – 60 keV; Feroci et al. 2007), the Mini-calorimeter (MCAL, sensitive in the range 0.35 – 100 MeV; Marisaldi et al. 2008; Fuschino et al. 2008; Labanti et al. 2009) with  $4\pi$  acceptance, and the anti-coincidence (AC) system (Tavani et al. 2009). The combination of the Tracker, MCAL, and the AC working together constitutes the  $\gamma$ -ray imager (GRID) capable of detecting  $\gamma$ -ray transients and GRB-like phenomena with a good sensitivity. The GRID has an instantaneous field of view (FoV) of a radius of  $70^\circ$  around pointing direction, while Super-A has a 2D-coded FoV region of radius  $\sim 32^\circ$ . The MCAL detector is equipped with a special triggering system capable of detecting burst events in the millisecond time range. MCAL detects MeV transients (e.g., gamma-ray bursts, GRBs) on timescales ranging from sub-milliseconds to hundreds of seconds.

AGILE data are transmitted to the ground at the ASI Malindi (Kenya) ground station, and delivered to the AGILE Data Center (ADC; part of the ASI Space Science Data Center). Scientific data are then processed by a fast dedicated pipeline which was recently enhanced for the search of electromagnetic counterparts of gravitational wave sources (Verrecchia et al. 2018; Ursi et al. 2019; Verrecchia et al. 2019). AGILE data processing can typically produce alerts for transient  $\gamma$ -ray sources and/or GRB-like events within 20 minutes – 2 hr from satellite on-board acquisition depending on orbital and satellite parameters (Pittori et al. 2013; Bulgarelli et al. 2014).

We report in this paper high-energy observations by AGILE of two repeating FRBs recently reported by CHIME (C19) which are characterized by small intrinsic DMs (among the smallest ever determined).

## 2. TWO REPEATING FRBS WITH SMALL INTRINSIC DM

Among the sample of the 8 repeating FRBs of C19, two have quite small intrinsic DMs: FRB180916.J0158+65 (Source 1), and FRB181030.J1054+73 (Source 2). Table 1 summarizes the characteristics of these repeating radio burst sources, providing the time and the measured radio fluences on millisecond timescales.

Source 1 is of particular interest because it emitted 10 bursts within a 6-month timescale with an average DM  $\sim 349 \text{ pc cm}^{-3}$ . Its position is near the Galactic plane at coordinates ( $l = 129.7^\circ$ ,  $b = 3.7^\circ$ ). The range of possible Galactic contributions to the dispersion measure,  $DM_{gal}$ , according to two different models (Cordes & Lazio 2002; Yao et al. 2017) is between 200 and  $325 \text{ pc cm}^{-3}$  (C19). The residual intrinsic DM can therefore be quite small. If Source 1 is located within or near our Galaxy, it should be at the edge of the Milky Way or in its halo (although the likelihood to detecting an active neutron star in the Galactic halo is expected to be low; Faucher-Giguère & Kaspi 2006; Olausen & Kaspi 2014; Cordes & Chatterjee 2019). Also if it is extragalactic, it might be in any case one of the nearest repeating FRBs. Assuming the intergalactic (IGM)-DM relation  $DM \simeq 900 z \text{ pc cm}^{-3}$  (McQuinn 2014), we obtain the maximum redshift  $z_{max} \sim 0.1$  for a maximum excess DM of  $100 \text{ pc cm}^{-3}$  (C19).

Source 2, located within an uncertainty region of 0.24 square degrees with centroid Galactic coordinates  $l = 133.4^\circ$  and  $b = 40.9^\circ$ , has the lowest overall DM value ever determined ( $DM = 103.5 \text{ pc cm}^{-3}$ ). The range of  $DM_{gal}$  for different models is between 32 and  $40 \text{ pc cm}^{-3}$ . The inferred redshift is therefore  $z < 0.023$ , which implies a luminosity distance less than 100 Mpc.

### 3. AGILE OBSERVATIONS

We searched in the recent AGILE archival data for possible exposures of the location regions of Source 1 and Source 2. AGILE is operating in spinning mode since 2009 with a revolution of its axis around the Sun-satellite direction every 7 minutes. This mode allows the AGILE/GRID to cover 80% of the sky more than 100 times a day. Gamma-ray exposures of any accessible field last  $\sim 2$  minutes for every satellite revolution with a typical flux sensitivity  $\sim 10^{-8} \text{ erg cm}^{-2} \text{ s}^{-1}$  above 30 MeV. Furthermore, AGILE is the only mission equipped with the on-board sub-millisecond triggering capability of AGILE/MCAL. This makes possible the detection of very fast events in the range 0.4–100 MeV (such as Terrestrial Gamma-ray Flashes detected in the sub-millisecond range; Tavani et al. 2011; Marisaldi et al. 2014).

Based on the FRB data of Table 1, we first verified the AGILE coverage at the times of the FRB occurrences. Depending on data availability, Earth occultation, and detector operations, we first determine for all interesting cases the proper exposure of the AGILE detectors (MCAL, GRID and Super-A) at the radio burst times ( $T_0$ ). It is possible that at  $T_0$  the event location is either occulted by the Earth, or it is inside the sky exclusion region in the solar/antisolar directions. We mark such cases with "NO" the entries of Table 1. We mark with "YES" cases for which the radio event is accessible by the AGILE detectors.

As reported in Table 1, MCAL had exposure for 8 bursts of Source 1; two of them were also in the GRID FoV, and none in the Super-A one. Figure 1 (right panels) shows the positions of two events (F and G of Table 1) of Source 1 and the simultaneous FoV of the GRID and Super-A at their respective  $T_0$ .

In these plots the FRB positions are marked by red stars, the blue line represents the edge of the GRID FoV, the purple circle the edge of Super-A FoV. Every event that falls between the center of the purple circle and the blue line is accessible by the GRID. In the left panels of Figure 1 we show the GRID and Super-A FoVs at  $T_0 - 100 \text{ s}$  for which the satellite had a better coverage of source position.

Regarding Source 2, both bursts were observed by MCAL but the GRID detector was completely occulted at  $T_0$ . In Figure 2, left top panel, is shown the AGILE exposures at  $T_0 - 100 \text{ s}$  (the best available exposure for this radio burst), and in the right top panel the exposures at  $T_0$ . For the second radio burst of Source 2 in the left bottom panel of Figure 2 is shown the exposure at  $T_0$  and in the right bottom panel the best available exposure at  $T_0 + 100 \text{ s}$ . Based on GRID exposures at the  $T_0$ 's, we focus our subsequent analysis to the bursts F and G of Source 1, and to both bursts (A and B) of Source 2.

#### 3.1. MCAL fluence upper limits

The AGILE/MCAL is a detector that operates with seven different trigger windows, from the unique sub-millisecond ( $\sim 300 \mu\text{s}$ ) timescale to a  $\sim 8 \text{ s}$  timescale. MCAL collects a stream of data whenever counts released in the detector exceeds a given threshold on a given timescale. The on-board hardware logic (acting on the shortest timescales  $0.293 \mu\text{s}$ ,  $1 \text{ ms}$ , and  $16 \text{ ms}$ ), issues a trigger

**Table 1.** Repeating FRBs and AGILE observations

| FRB parameters               |                  |                                 |                    | Event in the AGILE FoV |      |         |
|------------------------------|------------------|---------------------------------|--------------------|------------------------|------|---------|
| Label                        | Day<br>(yyymmdd) | Arrival time<br>(UTC @ 400 MHz) | Fluence<br>(Jy ms) | MCAL                   | GRID | Super-A |
| Source 1: FRB180916.J0158+65 |                  |                                 |                    |                        |      |         |
| A                            | 180916           | 10:15:19.8021                   | 2.3                | NO                     | NO   | NO      |
| B                            | 181019           | 08:13:22.7507                   | 2.7                | -                      | -    | -       |
| C                            | 181104           | 06:57:18.58524                  | 2.5                | YES                    | NO   | NO      |
| D                            | 181104           | 07:07:01.591                    | 2.0                | YES                    | NO   | NO      |
| E                            | 181120           | 05:56:06.23243                  | 1.8                | YES                    | NO   | NO      |
| F                            | 181222           | 03:59:23.2082                   | 27                 | YES                    | YES  | NO      |
| G                            | 181223           | 03:51:28.96040                  | 8.1                | YES                    | YES  | NO      |
| H                            | 181225           | 03:53:03.9260                   | 1.9                | YES                    | NO   | NO      |
| I                            | 181226           | 03:43:30.1074                   | 3.8                | YES                    | NO   | NO      |
| L                            | 190126           | 01:32:45.3289                   | 2.0                | -                      | -    | -       |
| Source 2: FRB181030.J1054+73 |                  |                                 |                    |                        |      |         |
| A                            | 181030           | 04:13:13.0255                   | 7.3                | YES                    | NO   | NO      |
| B                            | 181030           | 04:16:21.6546                   | 2.2                | YES                    | NO   | NO      |

**Notes:**

No data are available at 181019 and 190126  $T_0$ s. FRB parameters from C19.

whenever a fixed number of counts is exceeded. A software logic (acting on the longest timescales 64, 256, 1,024, and 8,192 ms), issues a trigger whenever the countrate level above the background exceeds a significance ( $n\sigma$ ) threshold. The total duration of the data acquisition following a trigger depends on the integration timescales and on the on-board trigger configuration. MCAL underwent different changes of the on-board configurations during its lifetime; information about the current (since August 2016) trigger configuration of MCAL can be found in [Ursi et al. \(2019\)](#).

As shown in Table 1 that 70% of Source 1 bursts and 100% of Source 2 bursts are inside the FoV of MCAL. Source 1 burst A is occulted by the Earth and there are no available data at the Source 1 burst B occurrence. No triggers were registered around  $T_0$ 's and no transients were thus recorded by MCAL. If MCAL is not triggered, ULs for the fluence can be obtained by evaluating the minimum detectable flux as a function of angle (based on the detector response matrix) as required by the on-board trigger logic at different timescales. MCAL therefore provides fluence ULs for the seven different timescales of the on-board trigger logic, for events that did not trigger the detector. As an example, in Figure 3 are reported the fluence ULs obtained by MCAL for the radio burst F of Source 1. Similar values are obtained also for burst G of Source 1 and for those of Source 2. The MeV-fluence ULs obtained for sub-millisecond and millisecond timescales (being of the order  $10^{-8}$  erg cm $^{-2}$ ) are particularly important, as we discuss below.

### 3.2. GRID observations of Source 1 (FRB 180916.J0158+65)

As reported in Table 1, GRID has exposure of burst F and G of Source 1 at  $T_0$ . The radio burst positions are inside the GRID FoV as shown in the right panels of Figure 1.

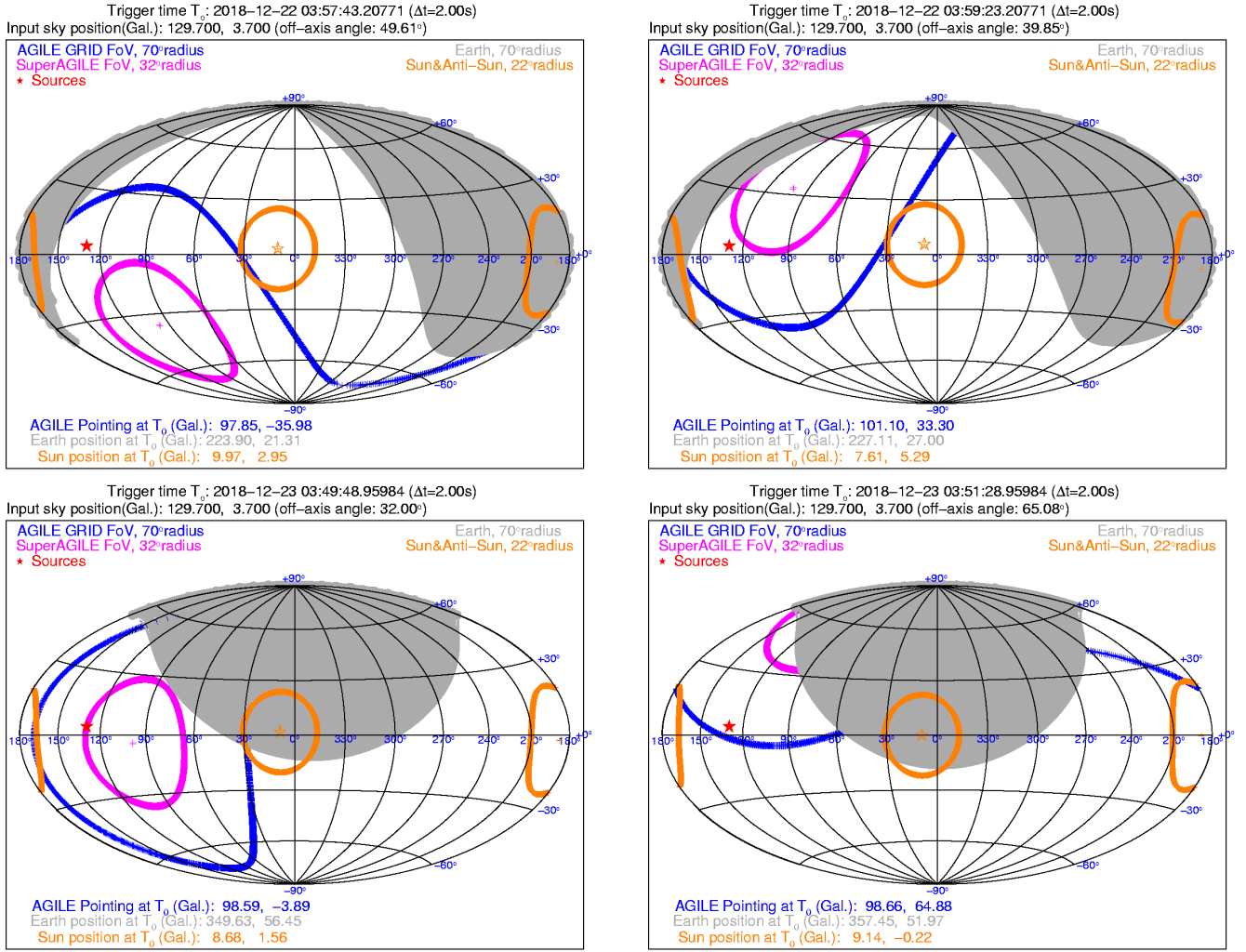


**Figure 1.** (*Top panels:*) AGILE exposure of burst F of Source 1 (FRB 180916.J0158+65) at  $T_0^{1,F} - 100$  s (left panel) and at  $T_0^{1,F}$  (right panel). Plots in Galactic coordinates. The position of the FRB is marked by a red star. The boundaries of the AGILE/GRID and Super-A FoVs are marked in blue and magenta color, respectively. (*Bottom panels:*) AGILE exposure of burst G of Source 1 at  $T_0^{1,G} - 100$  s (left panel) and at  $T_0^{1,G}$  (right panel). All images are ordered in time from left to right.

There is no known  $\gamma$ -ray source within a circle of radius 10 degrees, the usual AGILE maximum likelihood region of interest, at the position of the FRB. Since AGILE rotates every  $\sim 7$  minutes around a direction pointing at the Sun, the GRID obtained exposures of the source for each satellite revolution not affected by Earth occultation and/or SAA passages. We consider two types of analysis (as in Verrecchia et al. 2017): (1) the "GRB detection mode" for short integration times (see Giuliani et al. 2010) within the interval  $[0, +1000]$  s (times refer to  $T_0$ ) from 10 s to 1000 s integration times, in the 50 MeV - 10 GeV band; (2) the AGILE Maximum Likelihood analysis (Bulgarelli et al. 2012) for long integration times, ranging from 1 day to 100 days, in the 100 MeV - 10 GeV band.

The short exposures of Source 1, with 10, 100 and 1000 s integration times during the first passage on its position, allowed us to obtain the  $2\sigma$  flux ULs in the 50 MeV - 10 GeV band reported in Table 2;

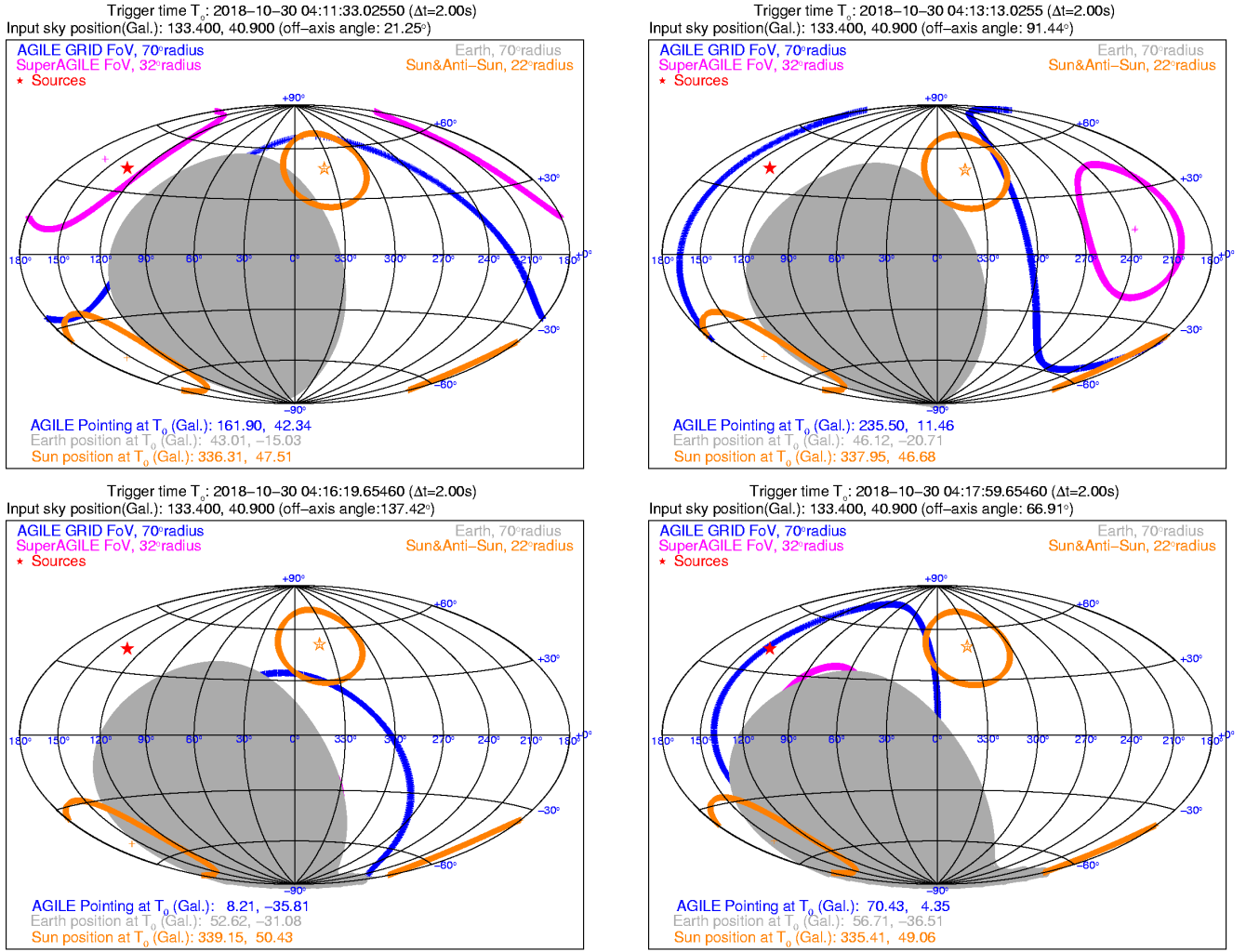


**Figure 2.** (*Top panels:*) AGILE exposure of burst A of Source 2 (FRB 181030.J1054+73) at  $T_0^{2,A} - 100$  s (left panel) and at  $T_0^{2,A}$  (right panel). Plots in Galactic coordinates. The position of the FRB is marked by a red star. The boundaries of the AGILE/GRID and Super-A FoVs are marked in blue and magenta color, respectively. (*Bottom panels:*) AGILE exposure of burst B of Source 2 at  $T_0^{2,B}$  (left panel) and at  $T_0^{2,B} + 100$  s (right panel). All images are ordered in time from left to right.

they range from  $1.69 \times 10^{-6}$  erg cm $^{-2}$  s $^{-1}$  to  $3.98 \times 10^{-7}$  erg cm $^{-2}$  s $^{-1}$ . The ULs values of burst F and G are compatible, with the exception of  $UL_{10s}^{1,F}$  that is  $\sim 4$  times smaller with respect  $UL_{10s}^{1,G}$ : this is because at  $T_0$  the source was at the edge of the GRID FoV which is moving away from the source region. Its effective exposure is lower than in the same interval for Burst F.

The long exposures (with integrations of 1, 10 and 100 days) lead to the  $2\sigma$  flux ULs (see Table 2) in the 100 MeV - 10 GeV band ranging from  $1.89 \times 10^{-10}$  erg cm $^{-2}$  s $^{-1}$  to  $2.64 \times 10^{-11}$  erg cm $^{-2}$  s $^{-1}$ . In Figure 4, we report our  $\gamma$ -ray ULs for Source 1 burst F only.

### 3.3. GRID observations of Source 2 (FRB 181030.J1054+73)

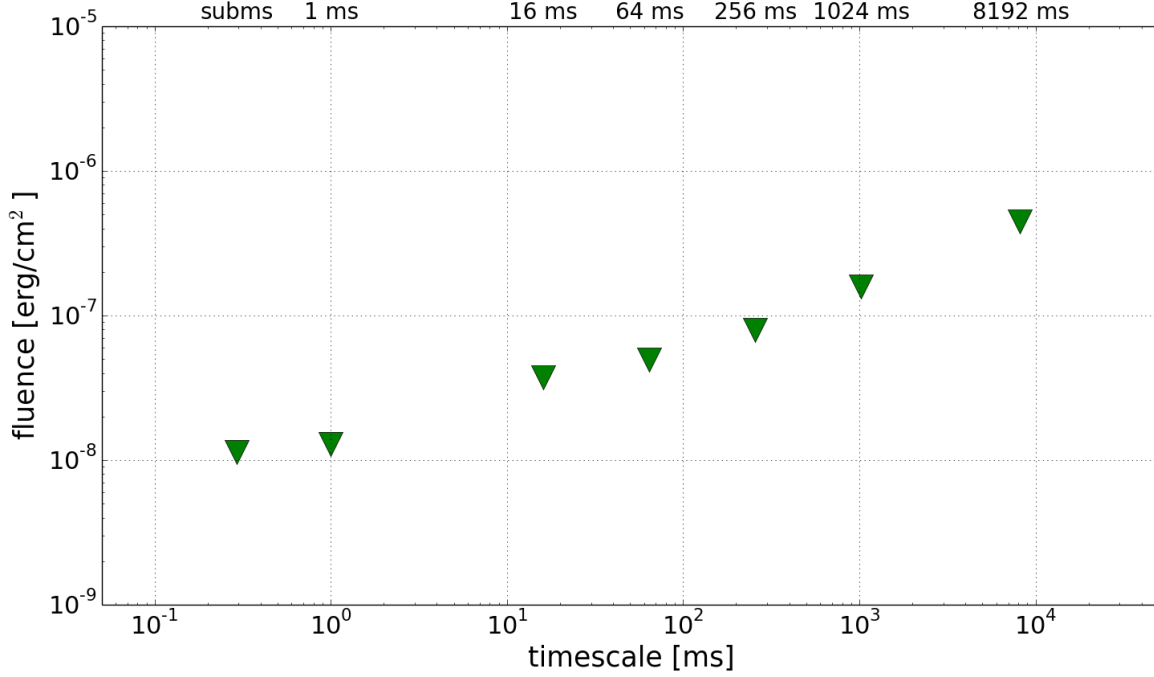


**Figure 3.** AGILE/MCAL fluence ULs in the energy range 0.4–1 MeV for the F radio burst of Source 1 as a function of integration timescales. Similar values are obtained for the burst G.

**Table 2.** AGILE/GRID flux ULs for the radio burst F, G of Source 1 and burst A of Source 2, as a function of integration timescales.

| Name       | $T_0 + 10^1 \text{ s}^{(a)}$      | $T_0 + 10^2 \text{ s}^{(a)}$      | $T_0 + 10^3 \text{ s}^{(a)}$ | $T_0 + 10^0 \text{ d}^{(b)}$ | $T_0 + 10^1 \text{ d}^{(b)}$ | $T_0 + 10^2 \text{ d}^{(b)}$ |
|------------|-----------------------------------|-----------------------------------|------------------------------|------------------------------|------------------------------|------------------------------|
| Source 1-F | $3.98 \times 10^{-7}$             | $3.60 \times 10^{-8}$             | $1.50 \times 10^{-8}$        | $1.90 \times 10^{-10}$       | $6.06 \times 10^{-11}$       | $2.64 \times 10^{-11}$       |
| Source 1-G | $1.69 \times 10^{-6}$             | $3.40 \times 10^{-8}$             | $1.60 \times 10^{-8}$        | $1.89 \times 10^{-10}$       | $5.92 \times 10^{-11}$       | $2.69 \times 10^{-11}$       |
| Source 2-A | $2.72 \times 10^{-7} \text{ (c)}$ | $4.67 \times 10^{-8} \text{ (c)}$ | $1.04 \times 10^{-8}$        | $3.39 \times 10^{-10}$       | $2.93 \times 10^{-11}$       | $1.18 \times 10^{-11}$       |

**Notes:**

(a,b):  $2\sigma$  flux ULs ( $\text{erg cm}^{-2} \text{s}^{-1}$ ) obtained for emission in the range 50 MeV–10 GeV for the short integration timescales and 100 MeV–10 GeV for the long ones, at each source positions.

(c): The first two ULs of Source 2 are evaluated on intervals [+390, +400] s and [+390, +490] s, respectively. These two intervals begin as the source begin to be exposed during the spinning rotation.

None of the two bursts of Source 2 are inside AGILE/GRID FoV at  $T_0$ , as shown in the top right panel and the bottom left panel of Figure 2. Also in this case, we split the analysis in short and long timescales, using the same integration times as in the previous case. Furthermore, due to the small amount of time between the two bursts ( $\sim$  few minutes), we made the analysis considering only the first repetition. The short exposures allowed us for this source to obtain the  $2\sigma$  flux ULs in the 50 MeV - 10 GeV band reported in Table 2), ranging from  $2.72 \times 10^{-7} \text{ erg cm}^{-2} \text{ s}^{-1}$  to  $1.04 \times 10^{-8} \text{ erg cm}^{-2} \text{ s}^{-1}$ . The 10 and 100 s integration ULs were evaluated on intervals [+390, +400] s and [+390, +490] s, respectively, when the source entered the GRID FoV. For longer exposures we

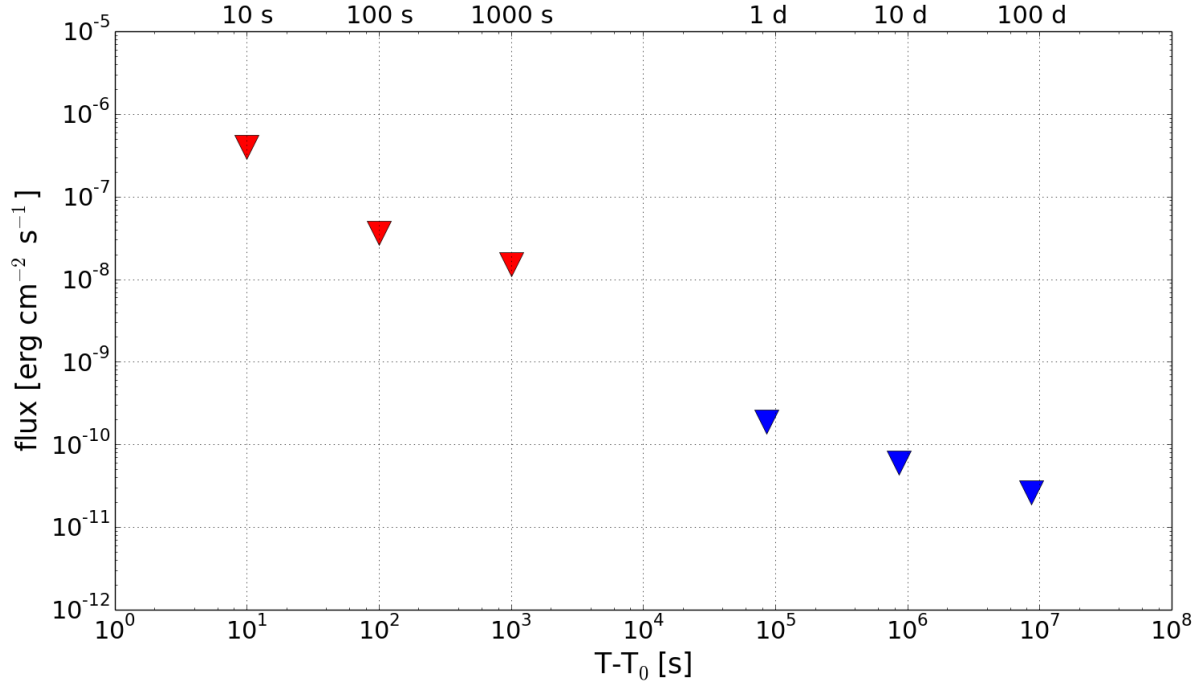


**Figure 4.** AGILE/GRID flux ULs for the F burst of Source 1 as a function of integration times. The energy ranges are  $50 \text{ MeV} < E < 10 \text{ GeV}$  for timescales 10,  $10^2$ ,  $10^3$ s (red markers), and  $100 \text{ MeV} < E < 10 \text{ GeV}$  for longer integrations (blue markers).

obtain ULs ranging from  $3.39 \times 10^{-10} \text{ erg cm}^{-2} \text{ s}^{-1}$  to  $1.18 \times 10^{-11} \text{ erg cm}^{-2} \text{ s}^{-1}$ , in the 100 MeV - 10 GeV energy band (see Table 2).

#### 4. DISCUSSION

The energy of the FRB radio burst emission is believed to be a small fraction of the total energy involved in any plasma configuration capable of radiating isotropically-estimated energies of  $10^{39}$  erg or larger for FRBs with large DMs (Cordes & Chatterjee 2019). If the large-DM FRBs are indeed at extragalactic distances, the underlying energy sources are most likely associated with phenomena involving compact objects, either neutron stars or black holes in peculiar states of emission. Therefore, constraining the energetics of the underlying plasma source for small-DM FRBs offers a unique way of exploring energy and luminosity ranges that are substantially smaller than those applicable to large-DM/extragalactic FRBs. Observed quantities depend on unknown beaming. In the following we assume isotropic emission for our estimates of energies and luminosities.

Our crucial fluence  $F'$  in the millisecond range is the typical AGILE/MCAL fluence UL obtained for several events of Table 1, that is  $F'_{\text{MeV}} = 10^{-8} \text{ erg cm}^{-2}$ . This value translates into an UL for the radiated energy into the MeV range,  $E_{\text{MeV},iso} = 4 \pi F' d_{100}^2 \simeq (10^{40} \text{ erg}) d_{100}^2$ , where  $d_{100} = d/100 \text{ kpc}$  with  $d$  the source distance from Earth. This value of  $E_{\text{MeV},iso}$  should be compared with the energy involved in the radio burst observation,  $E_{\text{radio},iso} \simeq (1.2 \cdot 10^{31} \text{ erg}) S_{\nu,Jy} \delta t_{ms} \Delta \nu_{\text{GHz}} d_{100}^2$ , where the measured FRB flux density in the radio band is  $S_{\nu,Jy}$  in units of Jansky,  $\delta t_{ms}$  is the temporal width in units of milliseconds, and  $\Delta \nu_{\text{GHz}}$  is the radio bandwidth in units of GHz. Note that events F and G of Source 1 have  $S_{\nu,Jy} \sim 10$ . If the two energies are compared for a time interval (e.g., milliseconds)

assumed to be the same for the radio and MeV emissions, the ratio  $E_{radio,iso}/E_{MeV,iso} \gtrsim 10^{-8}$  clearly indicates the marginal contribution of the radio emission from the point of view of the overall energetics for events that are expected to be detected in the MeV range. MCAL UL's for 1 - 10 s integrations are larger by more than one order of magnitude compared with that of millisecond timescales (see Figure 3), and the corresponding UL on the involved energy is  $E_{MeV,iso} \simeq (\text{a few } 10^{41} \text{ erg}) d_{100}^2$ .

MeV-radiated energies of order of  $10^{40} - 10^{41}$  erg are interesting for systems hosting a magnetar-like star, that is for stars whose outbursts are energized by either magnetic instabilities or by magnetospheric acceleration phenomena. The very large magnetic fields associated with magnetars (of the order of  $B_m \sim 10^{14} - 10^{16}$  G) in principle can be associated with maximal energies  $E_m \sim R_m^3 B_m^2 / 6 \simeq (2 \cdot 10^{49} \text{ erg}) B_{m,16}^2$ , with  $B_{m,16}$  the magnetar inner magnetic field in units of  $10^{16}$  G and where we assumed a magnetar radius  $R_m = 10^6$  cm. It is not clear how and when fractions of the total magnetic energy can be dissipated in special instabilities. The analysis of (Thompson & Duncan 1996) implies a timescale of  $\tau_a \sim 10^{11}$  s for ambipolar diffusion of the inner magnetar field, and therefore an average luminosity

$$L_a \sim E_m / \tau_a \sim (10^{38} \text{ erg}) E_{m,49} \tau_{a,11}^{-1} \quad (1)$$

where  $E_{m,49}$  is the maximal energy in units of  $10^{49}$  erg, and  $\tau_{a,11}$  is the diffusion time in units of  $10^{11}$  s. Smaller values of  $\tau_a$  (e.g. Beloborodov 2017) and/or of  $B_{m,16}^2$  imply larger/smaller average luminosities. We consider the luminosity  $L_a$  of Eq. 1 as a reasonable reference for comparison with our observations.

AGILE short time observations summarized in Table 1 and Figs. 1-3 severely constrain any flaring activity of a putative magnetar subject to sudden instabilities. Any MeV-radiated energy associated with simultaneous FRB activity is constrained to be less than  $E_{UL} \sim (10^{40} - 10^{41} \text{ erg}) d_{100}^2$ . When compared with the 2004 powerful flare of SGR 1806-20 that radiated  $E_{SGR} \simeq 2 \cdot 10^{46}$  erg in the MeV range (Palmer et al. 2005) our observations clearly exclude such an occurrence. If we use the observed example of  $10^{40} - 10^{41}$  erg in obtaining the fraction  $\xi$  of available magnetic energy being radiated into the MeV range, we deduce  $\xi \sim E_{MeV,SGR} / E_m \sim 10^{-3} B_{16}^{-2}$ . We therefore obtain the ULs on the flaring energies associated with the repeating FRBs of Table 1,  $E_* \sim E_{MeV,iso} / \xi \sim (10^{43} - 10^{44} \text{ erg}) B_{16}^{-2} d_{100}^2$ . These values exclude major magnetic flaring activity from magnetars with inner magnetic fields near  $10^{16}$  G. Therefore, either the magnetic field of the associated magnetars is substantially smaller than  $10^{16}$  G, or the strengths of the MeV flares are substantially smaller than those observed in the case of SGR 1806-20. Both of these possibilities are reasonable, and we consider these constraints an interesting outcome of our observations.

AGILE gamma-ray GRID observations of the locations of the repeating FRBs of Table 1 constrain also possible high-energy emission above 50 MeV on intermediate and long timescales as summarized in Table 2. If we consider the long timescale flux ULs for 100 day integrations, we obtain  $F_\gamma \sim (1 - 2) \cdot 10^{-11} \text{ erg cm}^{-2} \text{ s}^{-1}$ . Therefore, for the assumed FRB distance considered here, we obtain an UL on the isotropic luminosity emitted above 50 MeV,

$$L_{\gamma,UL} \simeq (1 - 2) \cdot 10^{37} d_{100}^2 \text{ erg s}^{-1}. \quad (2)$$

This luminosity should be compared with that of Eq. 1. A comparison of these two luminosities of the same order of magnitude suggests a not very constraining UL on the 50 MeV - efficiency  $\xi_{GeV} \lesssim 0.1$ . On the other hand, ULs of the type of Eq. 2 are the lowest ever obtained in the gamma-ray energy

range and constrain the flaring activity of the underlying source. For a source distance near 100 Mpc, our ULs imply  $E_{MeV,UL} \simeq 10^{46}$  erg and  $L_{\gamma,UL} \simeq (1 - 2) \cdot 10^{43}$  erg s<sup>-1</sup>.

## 5. CONCLUSIONS

Fast radio bursts continue to be puzzling with features that are not satisfactorily explained in current modelling of compact objects. A crucial diagnostic of the physical processes involved in FRBs is provided by X-ray and  $\gamma$ -ray simultaneous observations. In this paper we focused on two distinct FRB sources that erratically repeat and that have small intrinsic DM. From the hypothesis that the residual DM is directly related to distances, these two FRBs can be considered among the closest ever detected in the radio band. They are therefore the most interesting for constraining their high energy emission. Both Source 1 and Source 2 have been discussed within the hypothesis of an origin in our Galactic halo. If located well outside our Galaxy, an UL on their distances is of the order of 100 Mpc.

AGILE observations provide important constraints on the prompt (millisecond timescale) emission in the sub-MeV/MeV range, and exclude strong magnetar flares of the type of the 2004 event from SGR 1806-20. This is especially true for Galactic halo distances, but applies also to distances near 100 Mpc. Our UL of the MeV isotropic emitted energy at millisecond timescales  $E_{MeV,UL} \sim (10^{41} \text{ erg}) d_{100}^2$  severely constraints magnetar models of FRBs. For larger distances, the energy UL is less compelling, but in any case reaches values of the order of or less than the emitted MeV energy from the 2004 outburst of SGR 1806-20.

Furthermore, we constrain the persistent long timescale gamma-ray emission above 30 MeV from the repeating FRBs of Table 1. Our ULs of the average isotropic gamma-ray luminosity,  $L_{\gamma,UL} \simeq 10^{37} d_{100}^2 \text{ erg s}^{-1}$  exclude steady magnetar power to gamma-ray conversions of the order of 10% for sources in the Galactic halo. For more distant locations up to 100 Mpc, our ULs constrain the gamma-ray emitted power in a range substantially smaller than those detected by nearby blazars.

In conclusion, AGILE observations constrain the activity of the underlying energy source both on short and long timescales. Major flaring activities of the type of SGR 1806-20 are clearly excluded, with the AGILE MeV fluence ULs reaching values near 3 orders of magnitude less for nearby sources. The gamma-ray limits on the isotropic luminosity obtained above 30 MeV are somewhat less constraining. In any case, one can exclude the presence of an energy source at levels reported for different timescales in Table 2.

FRBs continue to be sources of great interest. More observations are needed to further constrain the emission process and the physical properties associated with the detected radio bursts. AGILE continues its observations of the gamma-ray sky, and will provide useful data for the search of FRB high-energy counterparts.

**Acknowledgments:** Investigation carried out with partial support by the ASI grant no. I/028/12/05.

## REFERENCES

- Barbiellini, G., Fedel, G., Liello, F., et al., 2002, NIM A, 490, 146
- Beloborodov, A. M., 2017, ApJL, 843, L26
- Bulgarelli, A., Chen, A. W., Tavani, M., et al. 2012, A&A, 540, A79
- Bulgarelli, A., Trifoglio, M., & Gianotti, F., 2014, ApJ, 781, 19
- Champion, D. J., Petroff, E., Kramer, M., et al., 2016, MNRAS, 460, L30
- Chatterjee, S., Law, C. J., Wharton, R. S., et al., 2017, Nature, 541, 58
- The CHIME/FRB Collaboration, Amiri, M., Bandura, K., Bhardwaj, M., et al. 2019a, Nature, 566, 230
- The CHIME/FRB Collaboration, Amiri, M., Bandura, K., Bhardwaj, M., et al. 2019b, Nature, 566, 235
- The CHIME/FRB Collaboration, Andersen, B. C., Bandura, K., Bhardwaj, M., et al. 2019c, arXiv e-prints, arXiv:1908.03507 (C19)
- Cordes, J. M., and Chatterjee, S., 2019, ARA&A, 119, 161101
- Cordes, J. M., & Lazio, T. J. W. 2002, arXiv preprint astro-ph/0207156
- Cunningham, V., Cenko, S. B., Burns, E., et al., 2019, ApJ, 879, 40
- Faucher-Giguère, C. A., & Kaspi, V. M., 2006, ApJ, 643, 332
- Feroci, M., Costa, E., Soffitta, P., et al., 2007, NIM A, 581, 728
- Fuschino, F., Labanti, C., Galli, M., et al. 2008, NIM A, 588, 17
- Giuliani, A., Fuschino, F., Vianello, G., et al. 2010, ApJL, 708, L84
- Hessels, J.W.T., Spitler, L. G., Seymour, A. D., et al., 2019, ApJ, 876L, 23
- Labanti, C., Marisaldi, M., Fuschino, F., et al. 2009, NIM A, 598, 470
- Lorimer, D. R., Faulkner, A. J., Lyne, A. G., et al., 2006, MNRAS, 372, 777
- Lorimer, D. R., Bailes, M., McLaughlin, M. A., Narkevic, D. J., & Crawford, F., 2007, Science, 318, 777
- Marcote, B., Paragi, Z., Hessels, J. W. T., et al., 2017, ApJL, 834, L8
- Marisaldi, M., Labanti, C., Fuschino, F., et al., 2008, A&A, 490, 1151
- Marisaldi, M., Fuschino, F., Tavani, M., et al., 2014, Journal of Geophysical Research (Space Physics), 119, 1337
- Martone, R., Guidorzi, C., Margutti, R., Nicastro, L., Amati, L., et al., 2019, arXiv e-prints, arXiv:1909.07165
- Michilli, D., Seymour, A., Hessels, J. W. T., et al., 2018, Nature, 533, 132
- McQuinn, M., 2014, ApJ, 780, L33
- Metzger, B. D., Margalit, B., and Sironi, L., 2019a, MNRAS, 485, 4091
- Olausen, S. A., & Kaspi, V. M., 2014, ApJS, 212, 6
- Petroff, E., Barr, E. D., Jameson, A., et al., 2016, PASA, 33, e045
- Palmer, D.M., Barthelmy, S., Gehrels, N., et al., 2005, Nature, 434, 1107
- Pittori, C., 2013, NuPhS, 239, 104
- Scholz, P., Bogdanov, S., Hessels, J. W. T., et al., 2017, ApJ, 846, 80
- Spitler, L. G., Scholz, P., Hessels, J. W. T., et al., 2016, Nature, 531, 202
- Tavani, M., Barbiellini, G., Argan, A., et al., 2009, A&A, 502, 995
- Tavani, M., Marisaldi, M., Labanti, C., et al., 2011, Physical Review Letters, 106, 018501
- Thompson, C. & Duncan, R. C., 1996, ApJ, 473, 322
- Ursi, A., Tavani, M., Verrecchia, F., et al., 2019, ApJ, 871, 27
- Verrecchia, F., Tavani, M., Donnarumma, I., et al., 2017, ApJL, 850, L27
- Verrecchia, F., Tavani, M., Bulgarelli, A., et al., 2019, RLSFN, doi:10.1007/s12210-019-00854-0
- Verrecchia, F., Tavani, M., Donnarumma, I., et al., 2018, IAUS, 338, 84
- Yao, J. M., Manchester, R.N., & Wang, N., 2017, ApJ, 835, 29